AIAA JOURNAL
Vol. 38, No. 10, October 2000

Thermal Buckling of Axially Precompressed Cylindrical Shells Irradiated by Laser Beam

Deng Keshun* and Ji Zheng†
Dalian University of Technology, 116023 Dalian, People's Republic of China
and
A. W. Davies‡ and F. W. Williams§
Cardiff University, Cardiff, Wales CF24 3TB, United Kingdom

When a powerful laser beam irradiates a thin-walled missile structure, the temperature of the irradiated region increases rapidly, which results in compressive thermal stresses being developed together with softening of the shell wall. Theoretical predictions of the buckling resistance of isotropic plates and shells, subjected to axial compression loading and a laser-induced nonuniform temperature field, have been developed and are presented. Material properties are assumed to be temperature dependent, which results in the thermal-buckling behavior being nonlinear with respect to temperature. Theoretical predictions are presented for a cylindrical shell subjected to axial compression loading and irradiated by a powerful laser beam. These show that the buckling resistance was significantly reduced by the combined action of axial compression loading and laser irradiation. Hence, it is likely that sudden buckling-induced failure may occur that can cause failure of highly optimized, lightweight cylindrical shells.

I. Introduction

THERMAL-BUCKLING behavior of structures is an important topic in the design of ballistic and cruise missiles. When a missile is subjected to a localized temperature field and free thermal expansion of its thin-walled components is restricted, or when spatially nonuniform heating occurs, compressive thermal stresses develop that can cause buckling-driven failures when the temperature field intensity increases sufficiently. One source of high-intensity nonuniform heating that is receiving serious consideration in the design of missile structures and missile defense systems is laser beam irradiation.

When a thin-walled missile structure is irradiated by a powerful, long-duration pulse laser beam over a relatively large section of the missile, the temperature of the irradiated region increases rapidly, which results in compressive thermal stresses being developed together with softening of the shell wall. When these two effects are superimposed on a system of preexisting compressive stresses in a highly optimized, lightweight missile structure, sudden buckling-induced failure of the missile may occur. The laser power density required for such a failure to occur is far smaller than the density required for comparable local failures such as spallation, melting, ablation vaporization, and punching.[1] Consequently, research into this topic is important to the design of missiles and missile defense systems.

Numerous theoretical and experimental studies have been carried out on the bifurcation buckling analysis of thermally loaded plates and shells having temperature-independent material properties. These analyses typically address the behavior of plates[2–5] and shells[6–9] having simple geometries, boundary conditions, and temperature fields. Practical engineering structures are often more complex, but these simple analyses can highlight important behavioral trends. Thermal-buckling induced failure of laser irradiated structures has received only modest attention.[10] Chen and Li[10] conducted an experimental study on the thermal-buckling failure of circular cylindrical shells that were loaded by a nondestabilizing uniform axial compression load and irradiated by a long-pulse, high-intensity laser beam. However, the experimental results exhibited a great amount of scatter, which suggests that the quality of the experimental data is poor.

Material properties, such as Young's modulus, Poisson's ratio, and the coefficient of thermal expansion, are essentially nonlinearly dependent on temperature. Theoretical predictions of the thermal-buckling resistance of cylindrical shells that exhibit such temperature-dependent material properties[11] are typically lower than when the temperature dependency is ignored.[4,6–9,12–14]

In the present study, a bifurcation buckling analysis procedure is presented for isotropic plates and shells that are subjected to an axial compression load and a laser-induced nonuniform temperature field. The axial compression load replicates the forces developed in a missile structure as a result of engine thrust and is treated as a steady-state, nondestabilizing loading condition that exists prior to laser irradiation. Material properties are assumed to be temperature dependent to account for the temperature fields produced by a long-duration, high-intensity laser pulse that acts over a relatively large region of a missile structure. Because the stiffness of the plate or shell depends on the intensity of the temperature field, the buckling analysis is manifested as a bifurcation from a nonlinear prebuckling solution path.

To validate the proposed analysis procedure, theoretical predictions have been compared with analytical solutions for annular, circular, and square plates subjected to thermal and compression loading. Numerical results are also presented for the thermal buckling of an axially precompressed cylindrical shell irradiated by a powerful laser beam, which show that the buckling resistance is significantly reduced by the combined action of local thermal stresses and material softening in the irradiated region.

II. Thermal-Buckling Analysis

In the present study, a bifurcation buckling analysis for cylindrical shells subjected to thermal and axial loads is formulated using the equations of classical, uncoupled thermoelasticity. Variations in the temperature field caused by small strains and moderate rotations of the shell are neglected. This simplification allows the temperature field to be calculated independently of shell deformations and to be used directly in the buckling analysis. The temperature field[11] can be expressed as

Received 26 November 1997; revision received 30 November 1998; accepted for publication 16 February 2000.

*Professor, Research Institute of Engineering Mechanics; currently Visiting Professor, Division of Structural Engineering, Cardiff School of Engineering, Cardiff University, Cardiff, Wales CF24 3TB, United Kingdom.

†Associate Professor, Research Institute of Engineering Mechanics; currently Visiting Professor, Division of Structural Engineering, Cardiff School of Engineering, Cardiff University, Cardiff, Wales CF24 3TB, United Kingdom.

‡Lecturer, Division of Structural Engineering, Cardiff School of Engineering.

§Professor and Head of Division of Structural Engineering, Cardiff School of Engineering.

$$C\rho\frac{\partial T}{\partial t} = \lambda\left(\frac{\partial^2 T}{\partial x^2} + \frac{\partial^2 T}{\partial y^2} + \frac{\partial^2 T}{\partial z^2}\right) + w \tag{1}$$

where T is the temperature, t is time, C is the specific heat, ρ is the material density, λ is the heat conductivity coefficient, w is the intensity of the heat source, and x, y, z is the Cartesian axis system. The intensity of the heat source[11] w can be written as

$$w = (1 - \xi) \cdot Q \cdot p(r) \cdot \cos\theta / h \tag{2}$$

where ξ is the reflection coefficient for laser beams on a cylindrical shell surface, Q is the incident laser intensity, $p(r)$ is the distribution function of Q, r is the radius from the center of the laser beam, θ is the angle between the internal normal line and the incident ray of the laser beam, and h is the shell thickness. Note that w and θ vary within the laser spot.

Because the shell is assumed to have temperature-dependent material properties, the bifurcation analysis presented is for a nonlinear prebuckling solution path, which means that the stiffness of the shell is a function of the intensity of the thermal loading. Two load parameters are used to describe the loading systems, an active thermal loading parameter τ and a passive axial loading parameter p. The axial loading is assumed to exist prior to thermal loading and to have a magnitude that corresponds to a point on the prebuckling solution path; that is, it corresponds to a subcritical equilibrium state. Thus, the passive nondestabilizing axial loads are introduced into the analysis as stiffnesslike terms that remain constant as the intensity of the thermal loading is increased.

A bifurcation point on the nonlinear, prebuckling solution path is obtained by finding the singular point of the global nonlinear finite element equations[15] that are given by

$$[K]\{u\} = \{f\} \tag{3}$$

where $[K]$ is the global stiffness matrix, which is dependent on the displacement and the magnitude of the axial and thermal loads; $\{u\}$ is the global nodal displacement vector; and $\{f\}$ is the global nodal force vector, which can be written as

$$\{f\} = \{f_P\} + \{f_T\} \tag{4}$$

where $\{f_P\}$ and $\{f_T\}$ are the axial and thermal components, respectively. The equivalent nodal forces for the thermal load used to construct $\{f_T\}$ are presented in the Appendix.

The singular points of the global nonlinear finite element equations are obtained by solving the homogeneous problem,[15] given by

$$[K_b] + [K_g]\{u\} = \{0\} \tag{5}$$

where $[K_b]$ is the global bending stiffness matrix and $[K_g]$ is the global geometric stiffness matrix that accounts for the interaction between membrane stresses and through-thickness deformations of the shell wall. In the present study $[K_b] = [K_b(\tau)]$ because of the temperature-dependent material properties and $[K_g] = [K_g(\tau, p)]$ because membrane stresses are produced by both loading systems. The geometric stiffness matrix can be partitioned into corresponding axial and thermal loads, as follows:

$$[K_g(\tau, p)] = [K_{g\tau}(\tau)] + [K_{gp}(p)] \tag{6}$$

Using this simplification, the bifurcation equations become

$$([K_b(\tau)] + [K_{g\tau}(\tau)] + [K_{gp}(p)])\{u\} = \{0\} \tag{7}$$

The bifurcation point of Eq. (7) depends on the active thermal loading parameter τ. Thus, Eq. (7) may be rewritten as

$$([K_b(\tau)] + [K_{gp}(p)] + \lambda[K_{g\tau}(\tau)])\{u\} = \{0\} \tag{8}$$

or

$$([K_b(\tau)] + [K_{gp}(p)])\{u\} = -\lambda[K_{g\tau}(\tau)]\{u\} \tag{9}$$

in which $\lambda = \lambda(\tau)$ and a value of $\lambda = 1$ corresponds to a bifurcation point where $\tau = \tau_{cr}$.

Solution of the bifurcation equations requires an incremental process in which the active thermal loading parameter is the independent variable. The procedure used in the present study consists of the following four steps:

1) The governing nonlinear finite element equation [Eq. (3)] is solved for an initial state of thermal loading. Then, the bifurcation equations [Eqs. (8) and (9)] are solved to determine whether the nonlinear solution corresponds to a critical value of the active, thermal loading parameter τ_1.

2) The value of the smallest eigenvalue τ_1 obtained from the solution of Eqs. (8) and (9) is used to investigate the inequality $|\lambda(\tau_1) - 1.0| < \varepsilon$, where ε is a small proximity tolerance. If the inequality is satisfied, the active thermal loading parameter corresponds to a bifurcation point on the solution path and $\tau_{cr} = \tau_1$. Otherwise, proceed to steps 3 and 4.

3) If the value of the smallest eigenvalue τ_1 obtained from the solution of Eqs. (8) and (9) satisfies the inequality $\lambda(\tau_1) > 1.0$, then the thermal loading parameter $\tau_1 < \tau_{cr}$ and no lower bound λ has been found. The golden section search[16] is then used between τ_1 of the current step and zero or τ from the last iteration to modify the incremental temperature load. Values of E, μ, and α should also be modified according to the revised temperature. Return to step 1 and continue the incremental process.

4) If the value of the smallest eigenvalue τ_1 obtained from the solution of Eqs. (8) and (9) satisfies the inequality $\lambda(\tau_1) < 1.0$, then the thermal loading parameter $\tau_1 > \tau_{cr}$ and a lower bound λ already exists (the lower bound is zero at the first iteration). The next temperature loading is calculated by the bisection, that is, interval halving, method between τ_1 and τ. Values of E, μ, and α should also be modified according to the revised temperature. Return to step 1 and continue the incremental process.

III. Comparison of Theoretical and Analytical Solutions

To validate the proposed bifurcation buckling analysis procedure, numerical results for three thermal buckling plate problems are compared with analytical solutions.

A. Annular Plate with Clamped Boundaries

Consider an annular plate with clamped boundaries of internal radius $a = 50.0$ cm, external radius $b = 100.0$ cm, thickness $h = 1.0$ cm, Young's modulus $E = 107$ GPa, Poisson's ratio $\mu = 0.333$, and coefficient of thermal expansion $\alpha = 9.375 \times 10^{-6}/°C$, subjected to a temperature load, given by

$$T(r) = T_a + K \cdot \ln(a/r) \tag{10}$$

in which $T_a = T(a) = 1.0$, $T_b = T(b) = 1.0$, $K = (T_a - T_b)\ln(a/b) = \ln(0.5)$, and r is the radial distance. Here 576 triangular shell elements and 336 nodes were used to model the annular plate. The theoretical critical buckling temperature $\tau_{cr} = 104.1°C$ shows good agreement with the result presented by Tani,[12] in which $\tau_{cr} = 103.4°C$, when we assume that the effect of temperature on material properties is ignored.

The effect of temperature on the material properties of carbon steel[17] with a Young's modulus $E = 211$ GPa, Poisson's ratio $\mu = 0.3$, and coefficient of thermal expansion $\alpha = 10.76 \times 10^{-6}/°C$ is shown in Table 1 (μ is assumed to remain constant). The theoretical critical buckling temperature τ_{cr}, with annular plate thickness $h = 1.5$ cm, $T_a = T(a) = 1.0$, and $T_b = T(b) = 0.0$, is presented in Table 2. When the effect of temperature on material properties is included in the numerical analysis, the critical buckling temperature τ_{cr} is approximately 15% lower than when it was ignored.

B. Circular Plate with Clamped Boundaries Under Local Temperature Load

Consider a circular plate with clamped boundaries of radius $a = 100.0$ cm, thickness $h = 5.1824$ cm, Young's modulus $E = 211$ GPa, Poisson's ratio $\mu = 0.3$, and coefficient of thermal expansion $\alpha = 10.76 \times 10^{-6}/°C$. Here 904 triangular shell elements

Table 1 Temperature-dependent material properties of carbon steel

T, °C	E, GPa	α, 10^{-6}/°C
0	211	10.76
20	210	——
100	206	11.53
200	201	12.25
300	189	12.90
400	184	13.58
450	178	13.93
500	168	14.22
550	156	14.42
600	141	14.62

Table 2 Annular plate

Temperature effects on E and α	Critical temperature, T_{cr}, °C
Ignored	503.07
Included	429.46

Table 3 Circular plate

Temperature effects on E and α	Critical temperature T_{cr}, °C
Ignored	491.93
Included	396.45

and 447 nodes were used to model the circular plate. If we define a temperature load parameter $\tau = 12(1+\mu)\alpha T a^2/h^2$, and a uniform temperature load acts on the whole plate, the theoretical critical buckling temperature $\tau_{cr} = 14.7524$°C when the effect of temperature on material properties is ignored. This shows close agreement with the critical buckling temperature $\tau_{cr} = 14.6869$°C presented by Kanaka.[5]

Furthermore, consider that a uniform temperature load T acts on the region $0 \le r \le a/2$, where r is the radial distance. The effect of temperature on the material properties[17] E and α is shown in Table 1 (μ is assumed to remain constant). The theoretical critical buckling temperatures τ_{cr} are presented in Table 3 and show that when the effect of temperature on material properties is included in the analysis, the critical buckling temperature τ_{cr} is reduced by approximately 19%.

C. Square Plate with Simple Boundary Conditions Under Longitudinal Compressive and Thermal Loading

A square plate of side length $a = 200.0$ cm, thickness $h = 2.0$ cm, Young's modulus $E = 211$ GPa, Poisson's ratio $\mu = 0.3$, and coefficient of thermal expansion $\alpha = 10.76 \times 10^{-6}$/°C has simple boundary conditions defined by $u \neq 0$, $v \neq 0$, $w = 0$, and $\theta_x \neq 0$ or $\theta_y \neq 0$ at the boundaries with $x = \pm a/2$ or $y = \pm a/2$, respectively. Cartesian coordinates x and y have their origin at the center of the plate. Because of symmetry of both the square plate and its buckling modes, the plate was modeled as a quarter plate using triangular shell elements in a 8×8 mesh. Three load cases were considered:

1) For a longitudinal uniform compressive load per unit width of N, solve for N_{cr}.

2) Solve for T_{cr} for a temperature loading T over a centrally positional square of side length 100 cm, where $-50 \le x, y \le 50$ cm, and $T = 0$°C elsewhere.

3) Find T_{cr} when $N = 4.0 \times 10^4$ N/cm is combined with the temperature loading defined in case 2.

Theoretical results for the three load cases are presented in Table 4. Good agreement was found between the theoretical critical compressive force N_{cr} and the analytical solution.[18] Furthermore, the critical compressive force N_{cr} for case 3 was approximately 53% smaller than the analytical solution for case 1, when the temperature loading T over a centrally positioned square was equal to 308.76°C.

Table 4 Square plate

Number of load cases	Numerical result	Analytical solution[18]
Uniform compression per width N_{cr}, kN/cm	60.988	61.026
Local uniform temperature rise T_{cr}, °C	335.20	——
$N = 4.0 \times 10^4$ N and local temperature rise T_{cr}, °C	308.76	——

Table 5 Temperature-dependent material properties of aluminum alloy

T, °C	E, GPa	μ	α, 10^{-6}/°C
0	70.0	0.350	22.00
100	65.1	0.355	23.60
200	57.5	0.360	25.20
300	37.0	0.365	26.80
400	20.0	0.370	28.40
500	15.0	0.375	30.00

IV. Thermal Buckling of Axially Precompressed Cylindrical Shell Irradiated by a Laser Beam

Numerical results using the proposed bifurcation buckling analysis procedure are compared with analytical and experimental results for a circular cylindrical shell of length $L = 12.3$ cm, diameter $D = 6.6$ cm, and uniform thickness $h = 0.018$ cm. The curved edges of the shell were clamped to restrain radial displacements and rotations of line elements perpendicular to the edges; in-plane displacements of the shell were unrestrained. The shell was made of an aluminium alloy of Young's modulus $E = 70$ GPa, Poisson's ratio $\mu = 0.35$, and coefficient of thermal expansion $\alpha = 22.0 \times 10^{-6}$/°C. The effect of temperature on the material properties of the aluminium alloy is presented in Table 5. (Young's modulus E comes from Fig. 3 of Ref. 1, and Poisson's ratio μ and the coefficient of thermal expansion α come from Ref. 11.)

Results are presented, first, for a shell that is loaded by a uniform uniaxial compression load P, which is used to determine the critical axial load P_{cr} without temperature loading. Second, thermal buckling results are presented for a shell that is subjected to nondestabilizing uniform uniaxial compression loads, before heating by a high-intensity, long-pulse laser beam with a relatively large region or spot of contact. The spot is essentially a region with a near-circular boundary of diameter $d = 4.8$ cm that is located at midlength of the shell, as shown in Fig. 1. The incident laser intensity $Q = 410$ W/cm^2, and the reflection coefficient of the cylindrical shell surface $\xi = 0.96$. The distribution function $p(r)$ of the laser beam intensity over the spot was approximated by a Gaussian distribution, such that

$$p(r) = \exp[-r^2/(2\zeta^2)] \tag{11}$$

in which $\zeta = d/4$ and r is the radial distance from the center of the laser beam.

Because heating occurs over a localized spot, the temperature field can be approximated to be a nearly square region of side length $l = 7.2$ cm, as shown in Fig. 1. This nearly square region and the spot it contains control the configuration of the finite element meshes used in the numerical study. Triangular shell elements were used to model the nearly square region; the remainder of the shell was modeled with rectangular shell elements.

Three finite element meshes were used to determine the linear bifurcation buckling load P_{cr} of the shell subjected to a uniform uniaxial compression load only. These meshes are shown in Fig. 2 and possess an irregular mesh distribution to facilitate thermal-buckling analyses. Mesh 1 has 1400 nodes and 1152 triangular and 784 rectangular shell elements. Similarly, mesh 2 has 2230 nodes and 1760 triangular and 1300 rectangular shell elements. Finally, mesh 3 has 3132 nodes and 2496 triangular and 1824 rectangular shell elements. The linear bifurcation buckling loads obtained with these meshes are presented in Table 6, together with the analytical solution given by Timoshenko and Gere[18] and the experimental results.[10] Comparison of these results shows a difference of approximately 50, 16.7,

and 2.6% between the results obtained from meshes 1, 2, and 3, respectively, and the analytical solution. However, the numerical and analytical results show poor agreement with the experimental results. This is attributed to the influence of initial imperfections and the unfavorable postbuckling characteristics that reduce the buckling resistance of cylindrical shells under axial compression.[19]

Although the numerical results presented in Table 6 indicate that mesh 3 should be used for thermal buckling analysis, mesh 2 was used to reduce computer time.

Consider a shell that is subjected to a nondestabilizing uniform uniaxial compression load, having various magnitudes, before heating. When we substitute the parameters just given into Eq. (2), the intensity of the laser beam source w is given by

$$w = 911.11 \times \exp(-0.3472r^2)\cos\theta \tag{12}$$

where $\cos\theta = 1$ at the center of the spot. Figure 3 illustrates the temperature distribution T_0 of the nearly square region containing the circular laser spot at $t = 1.0$ s, obtained by using a time step of $\Delta t = 0.1$ s. In Fig. 3, the temperature of the contours are $(0.32 + 26.49i)$°C, and the central temperature is 291.71°C.

To find T_{cr} $(=\lambda_{cr}T_0)$ for any given axial load P, let P_{cr} be the critical axial load without temperature loading, which was calculated to be $P_{cr} = 7179$ N. Numerical results are presented in Table 7 for four nondestabilizing uniform, uniaxial compression loads P that exist before laser irradiation, that is, $P = cP_{cr}$ for $c = 0.0$, 0.3, 0.6, and 0.67. Results indicate that the buckling resistance of the axially pre-compressed cylindrical shell decreases with the intensity of laser irradiation, and that the critical axial load P_{cr} for the irradiation causing T_0 is 67.1% of that without laser irradiation. Furthermore, as the ratio of P/P_{cr} approaches unity, the critical temperature ratio T_{cr}/T_0 decreases to zero. Figure 4 illustrates the corresponding buckling modes for $c = 0.0$ and 0.671 (the angle of view is from a few degrees to the right of the laser beam), which shows that major buckling deformation takes place in the irradiated spot.

Table 6 Critical axial compressive load P_{cr} of a cylindrical shell

Finite element mesh number	Numerical	Analytical[9]	Experimental
1	4294	——	——
2	7179	8613	1860 ± 260
3	8396	——	——

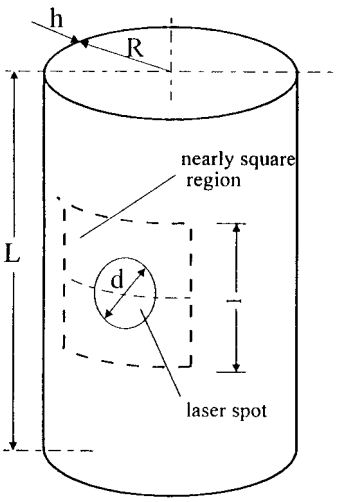

Location of laser spot

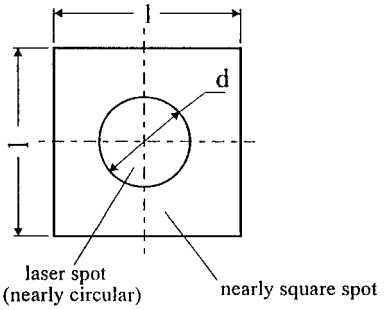

Laser spot

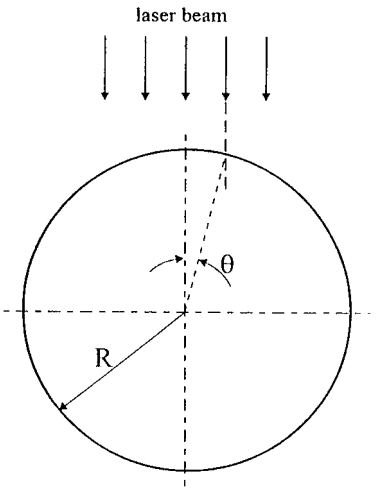

Incident angle of laser beam

Fig. 1 Cylindrical shell.

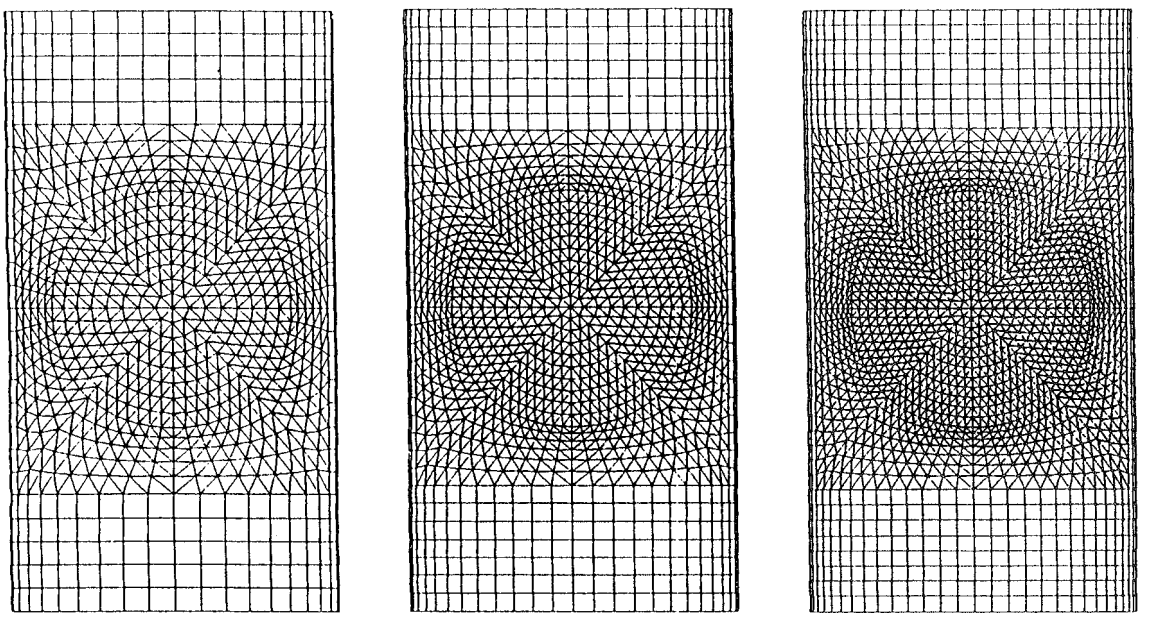

Mesh 1 Mesh 2 Mesh 3

Fig. 2 Finite element meshes.

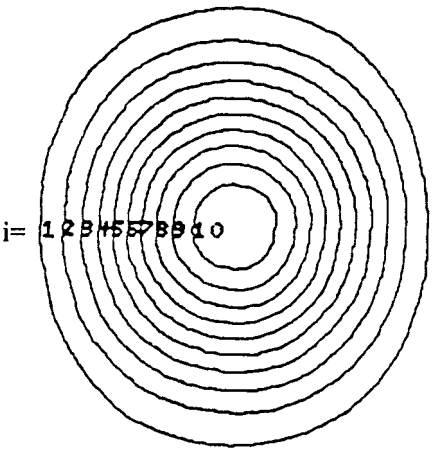

Fig. 3 Temperature field contours.

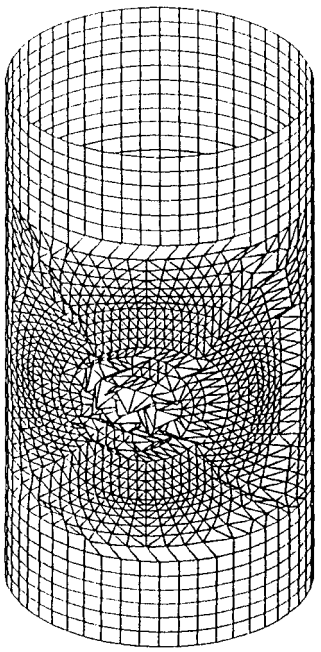

For $c = 0.0$ (load case 1)

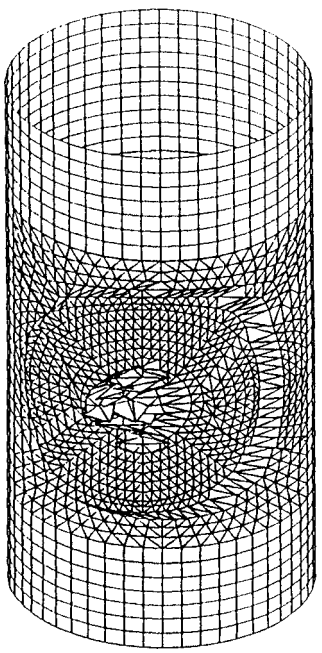

For $c = 0.671$ (load cases 4)

Fig. 4 Buckling modes.

Table 7 Critical preaxial compressive load P of a cylindrical shell subjected to laser irradiation

Axial load case number	$P = c \cdot P_{cr} = c \times 7179$, N	$T_{cr} = \lambda_{cr} \times T_0$, °C
1	$0.0 \times P_{cr}$	$1.21252 \times T_0$
2	$0.3 \times P_{cr}$	$1.12685 \times T_0$
3	$0.6 \times P_{cr}$	$1.02443 \times T_0$
4	$0.671 \times P_{cr}$	$0.99980 \times T_0$

V. Conclusions

Theoretical predictions have been developed for the buckling resistance of isotropic plates and shells subjected to axial compression loading and a laser-induced nonuniform temperature field. Laser irradiation produces high temperatures and a high-temperature gradient in the structure, which results in thermal softening and local compressive stresses in the spot zone. The thermal buckling analysis presented in this paper is, therefore, nonlinear with respect to temperature. Theoretical predictions of buckling resistance correlated closely with the analytical solutions for annular, circular, and square plates subjected to thermal and compression loading and having temperature-independent material properties. When the effect of temperature on material properties was included in the analyses, the critical buckling temperature τ_{cr} was significantly lower. Numerical results are presented for a cylindrical shell, having temperature-dependent material properties, subjected to axial compression loading, and irradiated by a powerful laser beam. The buckling resistance of the cylindrical shell was significantly reduced by the combined action of axial compression loading and laser irradiation. Results indicate that the critical axial load P_{cr} was 67.1% of that without laser irradiation. Therefore, it is likely that sudden buckling-induced failure may occur that can cause failure of highly optimized, lightweight cylindrical shells.

Appendix: Equivalent Nodal Forces for Thermal Loading

Thermal loads are transformed into nodal forces in the finite element analysis. The thermal load T, that is, the temperature difference, is assumed to be distributed uniformly through the thickness of plates or shells. The thermal load $T = T(x, y)$ is assumed to be a function of the Cartesian coordinates x and y. A normal strain αT will take place due to the thermal load T if the plate is unrestrained; otherwise (as is assumed in this paper), thermal stress will be generated.

The stress–strain relationship within the plate can be expressed as

$$\{\sigma\} = [\tilde{D}](\{\varepsilon\} - \{\varepsilon_T\}) \tag{A1}$$

in which $\{\sigma\}$ and $\{\varepsilon\}$ are given by

$$\{\sigma\} = \{\sigma_x \quad \sigma_y \quad \tau_{xy}\}^T, \qquad \{\varepsilon\} = \{\varepsilon_x \quad \varepsilon_y \quad \gamma_{xy}\}^T$$

$$\{\varepsilon_T\} = \alpha T\{1 \quad 1 \quad 0\}^T$$

$$[\tilde{D}] = \frac{E}{1-\mu^2}\begin{bmatrix} 1 & \mu & 0 \\ \mu & 1 & 0 \\ 0 & 0 & (1-\mu)/2 \end{bmatrix} \tag{A2}$$

In an element, the nodal force $\{F\}^e$ in the local Cartesian coordinate system that corresponds to mechanical loads can be written as

$$\{F\}^e = \iint [B]^T \{\sigma\} h \, dx \, dy \tag{A3}$$

where h is the plate thickness and $[B]$ is the strain-displacement matrix, in which $\{\varepsilon\}^e = [B]\{\delta\}^e$, where $\{\delta\}^e$ is the nodal displacement vector of the element. Substituting Eq. (A1) into Eq. (A3) gives

$$\{F\}^e + \iint [B]^T [D]\{\varepsilon_T\}^e \, dx \, dy = [k]\{\delta\}^e \tag{A4}$$

where $[D] = h[\tilde{D}]$ and $[k]$ is the element stiffness matrix. The second term on the left-hand side of Eq. (A4) represents the temperature effect. By comparing Eq. (A4) with $\{F\}^e = [k]\{\delta\}^e$, which is associated with mechanical loading only, temperature loading can be converted to an effective nodal forces vector $\{R\}^e$, given by

$$\{R\}^e = \iint [B]^T [D]\{\varepsilon_T\}^e \, dx \, dy \tag{A5}$$

For triangular elements, $\{R\}^e$ can be expressed as

$$\{R\}^e = \{R_{1x} \quad R_{1y} \quad R_{2x} \quad R_{2y} \quad R_{3x} \quad R_{3y}\}^T = A[B]^T [D]\{\varepsilon_T\}^e \tag{A6}$$

in which A is the area of the triangular element and

$$\{\varepsilon_T\}^e = \alpha \bar{T}\{1 \quad 1 \quad 0\}^T \tag{A7}$$

where $\bar{T}$ is the average element nodal temperature loads T_i at nodes i $(=1, 2, 3)$, that is, $\bar{T} = (T_1 + T_2 + T_3)/3$. Similarly, for rectangular elements, $\{R\}^e$ can be expressed as

$$R^e = \{R_{1x} \quad R_{1y} \quad R_{2x} \quad R_{2y} \quad R_{3x} \quad R_{3y} \quad R_{4x} \quad R_{4y}\}^T \tag{A8}$$

where

$$\begin{aligned}
R_{1x} &= -(\alpha b/6)(D_{11} + D_{12})(2T_1 + 2T_2 + T_3 + T_4) \\
R_{1y} &= -(\alpha a/6)(D_{12} + D_{22})(2T_1 + T_2 + T_3 + 2T_4) \\
R_{2x} &= -R_{1x} \\
R_{2y} &= -(\alpha a/6)(D_{12} + D_{22})(T_1 + 2T_2 + 2T_3 + T_4) \\
R_{3x} &= (\alpha b/6)(D_{11} + D_{12})(T_1 + T_2 + 2T_3 + 2T_4) \\
R_{3y} &= -R_{2y}, \qquad R_{4x} = -R_{3x}, \qquad R_{4y} = -R_{1y}
\end{aligned} \tag{A9}$$

in which T_i is the element nodal thermal loads at nodes i $(=1, 2, 3, 4)$ and D_{11}, D_{12}, D_{22}, and D_{33} are the elements of the flexural rigidity matrix.

Acknowledgments

This work was supported by the National Natural Science Foundation of China and the Cardiff Advanced Chinese Engineering Centre at Cardiff University. The authors are grateful for the comments received from the reviewers.

References

[1]Chen, Y., "Dynamic Thermal Failure of Structures Under Laser Irradiation," *Proceedings of IUTAM Symposium on Impact Dynamics*, Peking Univ. Press, Beijing, 1994, pp. 92–104.

[2]Prabha, M. S. S., and Durvasule, S., "Thermal Buckling of Skew Plates," *Canadian Aeronautics and Space Journal*, Vol. 20, 1974, pp. 111–113.

[3]Li, S., and Cheng, C., "Thermal Buckling of Circular Annular Plate Under Complex Load," *Applied Mathematics and Mechanics*, Vol. 12, No. 3, 1991, pp. 279–286 (in Chinese).

[4]Tani, J., "Thermal Buckling of an Annular Plate with Axi-Symmetric Initial Deflection," *Journal of Applied Mechanics*, Vol. 45, Sept. 1978, pp. 693–695.

[5]Kanaka, K. R., and Venkateswara, G. R., "Thermal Post-Buckling of Circular Plates," *Computers and Structures*, Vol. 18, No. 6, 1984, pp. 1179–1182.

[6]Ross, B., Hoff, N. J., and Horton, W. H., "The Buckling Behaviour of Uniformly Heated Thin Circular Cylindrical Shells," *Experimental Mechanics*, Vol. 6, No. 11, 1966, pp. 529–537.

[7]Chang, L. K., and Card, M. F., "Thermal Buckling in Stiffened Cylindrical Shell," *Proceedings of the AIAA/ASME 11th Structural Dynamics and Materials Conference*, AIAA, New York, 1970, pp. 260–272.

[8]Bushnell, D., "Analysis of Ring-Stiffened Shells of Revolution Under Combined Thermal and Mechanical Loading," *AIAA Journal*, Vol. 9, No. 3, 1971, pp. 401–410.

[9]Bushnell, D., and Smith, S., "Stress and Buckling of Nonuniformly Heated Cylindrical and Conical Shells," *AIAA Journal*, Vol. 9, No. 12, 1971, pp. 2314–2321.

[10]Chen, Y., and Li, S., "Buckling Failure of Axially Precompressed Cylindrical Shell Irradiated by CW CO_2 Laser Beam," AIAA Paper 93-3231, July 1993.

[11]Ji, Z., Deng, K., Davies, A. W., and Williams, F. W., "Numerical Modelling of Thermal Destruction of Cylindrical Shells with Pre-Internal Pressure Under Laser Irradiation," *Computers and Structures*, Vol. 71, No. 4, 1999, pp. 359–370.

[12]Tani, J., "Elastic Instability of a Heated Annular Plate Under Lateral Pressure," *Journal of Applied Mechanics*, Vol. 48, June 1981, pp. 399–403.

[13]Shen, H. S., "Postbuckling Analysis of Orthotropic Rectangular Plates on Non-Linear Elastic Foundations," *Engineering Structures*, Vol. 17, No. 6, 1995, pp. 407–412.

[14]Shen, H., and Zhang, J., "Thermal Postbuckling Analysis of Rectangular Plates on Non-Linear Elastic Foundations," *Chinese Journal of Applied Mechanics*, Vol. 14, No. 1, 1997, pp. 29–35.

[15]Cook, R. D., *Concepts and Applications of Finite Element Analysis*, Wiley, New York, 1974.

[16]Himmelblau, D. M., *Applied Non-Linear Programming*, McGraw–Hill, New York, 1972, pp. 43, 44.

[17]Fan, Q., *Stress Analysis and Strength Design of the Pressure Vessels*, Beijing Atomic Energy Press, Beijing, 1979, pp. 94 and 447 (in Chinese).

[18]Timoshenko, S. P., and Gere, J. M., *Theory of Elastic Stability*, McGraw–Hill, New York, 1985.

[19]Budiansky, B., "Theory of Buckling and Postbuckling Behaviour of Elastic Structures," *Advances in Applied Mechanics*, Vol. 14, 1974, pp. 1–65.

G. A. Kardomateas
Associate Editor